PMAS
Proceedings of the Mongolian Academy of Sciences
Vol. 66 No 01(257) 2026
https://doi.org/10.5564/pmas.v66i01.5134

ARTICLE

A comparative study of polyaniline-based composites doped with two-dimensional and three-dimensional structured carbon: the potential of coal for supercapacitor electrodes

Bolormaa Burentogtokh, Bumaa Batsuren*, Nomin Bayansan and Sevjidsuren Galsan

Laboratory of Energy Research, Institute of Physics and Technology, Mongolian Academy of Sciences, Ulaanbaatar, Mongolia

ARTICLE INFO: Received: 25 Sep, 2025; Accepted: 19 Jan, 2026

Abstract: This work examined the properties of reduced graphene oxide (rGO) with a 2D structure and activated carbon (AC) with a 3D structure, both doped with polyaniline (Pani), and synthesized through the polymerization method. The crystal structure, morphology, and molecular structure were analyzed using XRD, SEM, and FTIR methods respectively. The electrochemical properties of the composites were evaluated using CV, GCD, and EIS. The energy storage device characteristics, such as energy density and power density, were calculated from an assembled electrochemical capacitor with a 1 cm² working electrode. From the GCD measurements, Pani/AC exhibited the highest specific capacitance of 181.9 F/g at a current density of 1 A/g, while Pani/rGO had a specific capacitance of 145.8 F/g. Additionally, Pani/AC demonstrated a high capacitance retention rate. An energy density of 3.6 Wh/kg at a power density of 500 W/kg was observed in the Pani/rGO//Pani/rGO symmetric supercapacitor at a voltage of 1 V and a current density of 1 A/g. An energy density of 6.5 Wh/kg at a power density of 600 W/kg was observed in the Pani/AC//Pani/AC symmetric supercapacitor at a voltage of 1.2 V and 1 A/g. The electrochemical performance results indicate that the Pani/rGO and Pani/AC composites are effective electrode materials for supercapacitors. Therefore, we suggest that activated Mongolian coal could be a suitable electrode material for supercapacitor applications.

Keyword: *Supercapacitor, polyaniline, activated carbon, reduced graphene oxide;*

INTRODUCTION

Nowadays, smart devices require an energy storage device with fast charge/discharge ability, high power and high energy density, long cycle life, and a wide temperature range; and supercapacitors can address this problem [1, 2]. A supercapacitor has a higher energy density than a conventional capacitor and a higher power density than a regular battery. However, the supercapacitors currently in wide use have several disadvantages, including high industrial costs, low energy densities, capacitance loss, and instability due to the electrode material. Carbonaceous materials (graphene, activated carbon, etc.), metal oxides (RuO2, MnO2, etc.), and conductive polymers (Pani, Ppy, etc.) are used as electrodes in supercapacitors [3]. In recent years, much research has been conducted on the use of composite materials, such as electrodes, to improve the properties of these materials [4-7].

***Corresponding author, email:** bumaab@mas.ac.mn https://orcid.org/0000-0003-4845-4223

The Author(s). 2026 Open access This article is distributed under the terms of the Creative Commons Attribution 4.0 International License (https://creativecommons.org/licenses/by/4.0/), which permits unrestricted use, distribution, and reproduction in any medium, provided you give appropriate credit to the original author(s) and the source, provide a link to the Creative Commons license, and indicate if changes were made.

Vol. 66 No 01(257) 2026
https://doi.org/10.5564/pmas.v66i01.5134

Among conductive polymers, polyaniline (Pani) has been extensively studied because of its unique structure, high electrochemical activity, and ease of synthesis. Pani has three oxidation states: fully reduced – leucoemeraldine; half-oxidized – emeraldine; and fully oxidized – pernigraniline. In the half-oxidized state, the emeraldine base acts as a semiconductor, whereas the protonated emeraldine salt shows higher conductivity. However, during the electrochemical redox reaction, the volume of Pani expands and its structure changes, resulting in poor conductivity, reduced specific surface area, and decreased cycle stability [8-11]. These issues can be addressed by doping Pani with carbon materials.

One of the many types of carbon - 2D graphene, is known for its high conductivity. However, the strong π-π bonds form agglomerations that cause a decrease in the specific surface area and conductivity. Moreover, the synthesis of 2D materialsis a complex process that requires advanced technology, which increases the material's cost. On the other hand, reduced graphene oxide (rGO) has less agglomeration due to the existence of oxygen; therefore, studies on Pani with reduced graphene oxide composites have been studied widely [12-15]. Nevertheless, agglomeration still exists the during synthesis, which requires a different doping material.

Another type of carbon, 3D activated carbon (AC), offers several advantages, such as a high specific surface area resulting from a 3D porous structure, abundant natural resources for material sourcing, ease of synthesis, and environmental friendliness [16-18]. It is believed that this porous structure can reduce the agglomeration of Pani and enhance its conductivity.

Therefore, in this study, Pani was synthesized by doping it with 2D-structured graphene oxide and with 3D-structured activated carbon. We compared their properties to determine whether activated carbon is comparable to 2D-structured materials. According to [19], the optimal mass ratio of Pani to 2D materials was determined to be 90:10. However, Pani-based composites with 3D materials have been comparatively less investigated than Pani with 2Dmaterials. In contrast, previous studies [16] on Pani/AC systems have reported significantly lower AC content due to the high surface area and porous structure. Furthermore, this study aimed to explore the basis for the potential use of coal as a source of activated carbon, as it is abundant in Mongolia, making it relatively inexpensive to put into economic circulation.

MATERIALS AND METHODS

Chemicals

Aniline (Ani), ammonium peroxydisulfate (APS), polyvinylidene fluoride (PVDF), and dimethylformamide (DMF) were purchased from Sigma-Aldrich. Reduced graphene oxide (rGO) powder and carbon black (CB) were obtained from Kaina Carbon New Materials Co., Ltd., China. Wood-based activated carbon (AC) was obtained from Shijiazhuang Hongsen Activated Carbon Co., Ltd.

Synthesis

The preparation process of the Pani/rGO composite with a mass ratio of m_{Pani}: m_{rGO}= 90:10 was synthesized through chemical polymerization. Briefly, Ani and APS were dispersed separately in 1M HCl. Then, rGO was added to the dispersed Ani solution and mechanically stirred for 5 hours at room temperature. For the Ani polymerization step, the APS solution was added gradually to the Ani + rGO mixture, which was then mechanically stirred for 12 hours at room temperature. The resulting solution was repeatedly washed with double-deionized water, filtered, and dried at 40°C for 24 hours. For comparison, pure Pani was prepared without rGO, and the Pani/AC composite had a mass ratio of m_{Pani}: m_{AC}= 99:1.

Characterization

A scanning electron microscope (SEM) Hitachi SU8000 with energy-

Vol. 66 No 01(257) 2026
https://doi.org/10.5564/pmas.v66i01.5134

dispersive X-ray spectroscopy (EDS) was used to examine the morphological properties of the samples and to perform elemental analyses. X-ray diffraction (XRD) patterns were obtained using a Maxima XRD-7000 diffractometer with CuKα radiation (λ=0.154 nm). A Shimadzu IR Prestige-21 spectrometer was used to record Fourier transform infrared (FTIR) spectra. N_2 adsorption-desorption was measured at 77 K with a HORIBA SA-9600 surface area analyzer.

Electrochemical measurements

Cyclic voltammetry (CV) and galvanostatic charge-discharge (GCD) tests were conducted using an Epsilon Eclipse potentiostat. A Powerstat-20 potentiostat was employed for electrochemical impedance spectroscopy (EIS) in the frequency range from 0.1 Hz to 10 kHz, with a DC bias of 0.5 V. Electrochemical measurements of the samples were performed in a 3-electrode setup. Ag/AgCl and Pt wires served as the reference and counter electrodes, respectively, and the electrolyte was a 1 M H_2SO_4 aqueous solution. The working electrode was prepared by mixing the active material CB and PVDF in a mass ratio of 80:10:10 with DMF to create a homogeneous slurry. This slurry was then applied to a stainless-steel surface and dried at 80 °C for 12 hours. Approximately 1.5 mg of slurry was loaded onto a 1 cm^2 active area.

RESULTS AND DISCUSSION

Figure 1a shows the surface morphology of Pani, which has a granular structure, approximately 5 μm in size. Figure 1b displays the layered structure of the Pani/rGO composite due to the sheet-like morphology of rGO. The Pani/AC composite (Figure 1c) displayed a porous morphology.

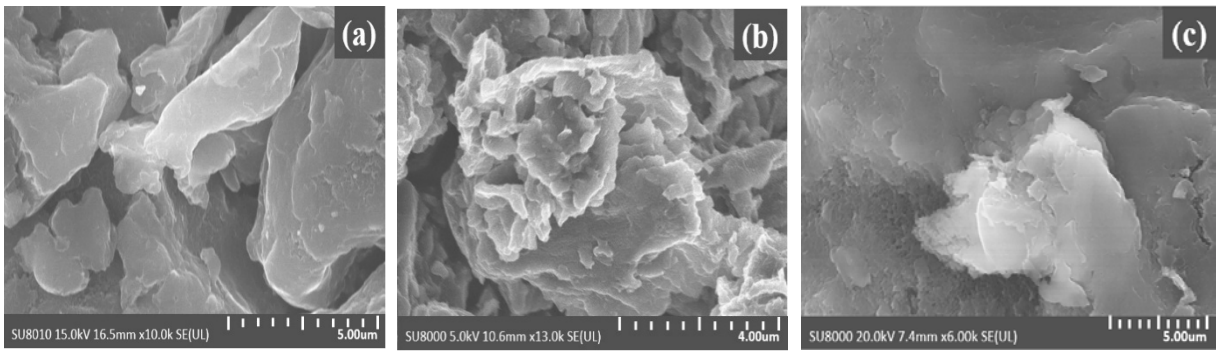

Figure 1. SEM images of (1a) Pani, (1b) Pani/rGO composites, and (1c) Pani/AC composites.

The results of the elemental analysis by SEM-EDS for all samples are shown in Table 1. As observed, when Pani was doped with rGO and AC, the carbon content increased, while the oxygen and nitrogen content decreased due to the influence of rGO and AC compared with Pani. The high chlorine and sulfur content in the Pani/AC composite results from residual Cl used in the synthesis of AC.

Table 1. EDS results for Pani, rGO, and the Pani/rGO composite.

Elements / Samples	Atomic, %				
	C	O	N	S	Cl
Pani	66.5	11.5	19.4	1.2	1.4
Pani/rGO	79.8	8.4	10.0	1.0	0.8
Pani/AC	79.2	3.5	4.2	4.8	8.3

Vol. 66 No 01(257) 2026
https://doi.org/10.5564/pmas.v66i01.5134

X-ray diffraction measurements were conducted to determine the crystal structures of Pani, the Pani/rGO, and the Pani/AC composites, and the results are shown in Figure 2a. The characteristic diffraction peaks of Pani appeared at 15.2°, 20.5°, and 25.5°, corresponding to the (011), (020), and (200) planes, respectively. For AC and rGO, two diffraction peaks were observed. A weak diffraction peak at $2\theta \approx 43.4°$ was detected for AC and rGO, attributed to the (100) plane of graphite, due to the minimal amount of the graphite phase [20]. For rGO, a diffraction peak at $2\theta \approx 25.5°$, corresponding to the (002) plane, yields an interlayer spacing of approximately 0.34 nm. In contrast, AC exhibits a broad (002) peak centered at $2\theta \approx 21.3°$, corresponding to a larger interlayer spacing of 0.42 nm, which confirms a disordered and amorphous structure compared with rGO. For the Pani/rGO composite, all the characteristic peaks of Pani and rGO were present. For the Pani/AC composite, all the characteristic peaks of Pani appeared, and no additional peaks were observed. The peak intensity at 25.4° was higher than at 20.5° for all samples, indicating a semicrystalline emeraldine salt state [21]

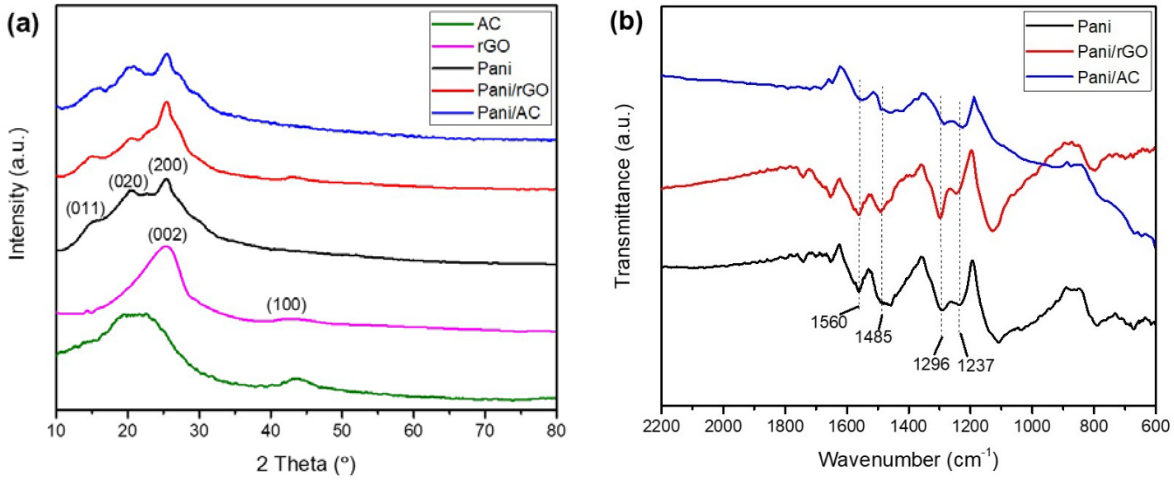

Figure 2. (2a) XRD spectra, and (2b) FT-IR spectra of Pani, Pani/rGO, and Pani/AC composites.

The FTIR spectra of Pani, the Pani/rGO composite, and the Pani/AC composite are shown in Figure 2b. In the spectrum of Pani, the absorption bands at 1561 and 1457 cm^{-1} correspond to benzenoid and quinoid ring vibrations respectively, indicating the structure of the obtained Pani. Spectra corresponding to C–N and C=N valence oscillations were recorded at 1290 cm^{-1} and 1237 cm^{-1} absorption bands, respectively, confirming the formation of the emeraldine salt state of Pani [22]. In the Pani/rGO and Pani/AC composites, the band around 1037 cm^{-1} decreased due to lower oxygen content [23].

The specific surface area was measured using the Brunauer-Emmett-Teller method. The Pani/rGO composite had a surface area of 12.8 m^2/g, which is three times lower than that of Pani (38.3 m^2/g) due to agglomeration and irregular morphology. The specific surface area of Pani/AC (18.4 m^2/g) is half that of Pani but higher than that of Pani/rGO composites because of the high porosity of AC.

The cyclic voltammograms of the Pani, Pani/rGO, and Pani/AC composite electrodes were recorded at a scan rate of 10 mV/s within the potential range of 0.2 V to 1 V, as shown in Figure 3. The graph shows that the area under the CV curves of the composites increased, indicating enhanced electrochemical activity. Additionally, two pairs of oxidation-reduction peaks appeared on the CV curves for the composites compared to pure Pani, demonstrating a strong synergistic effect between Pani and rGO, as well as between Pani and AC.

Vol. 66 No 01(257) 2026
https://doi.org/10.5564/pmas.v66i01.5134

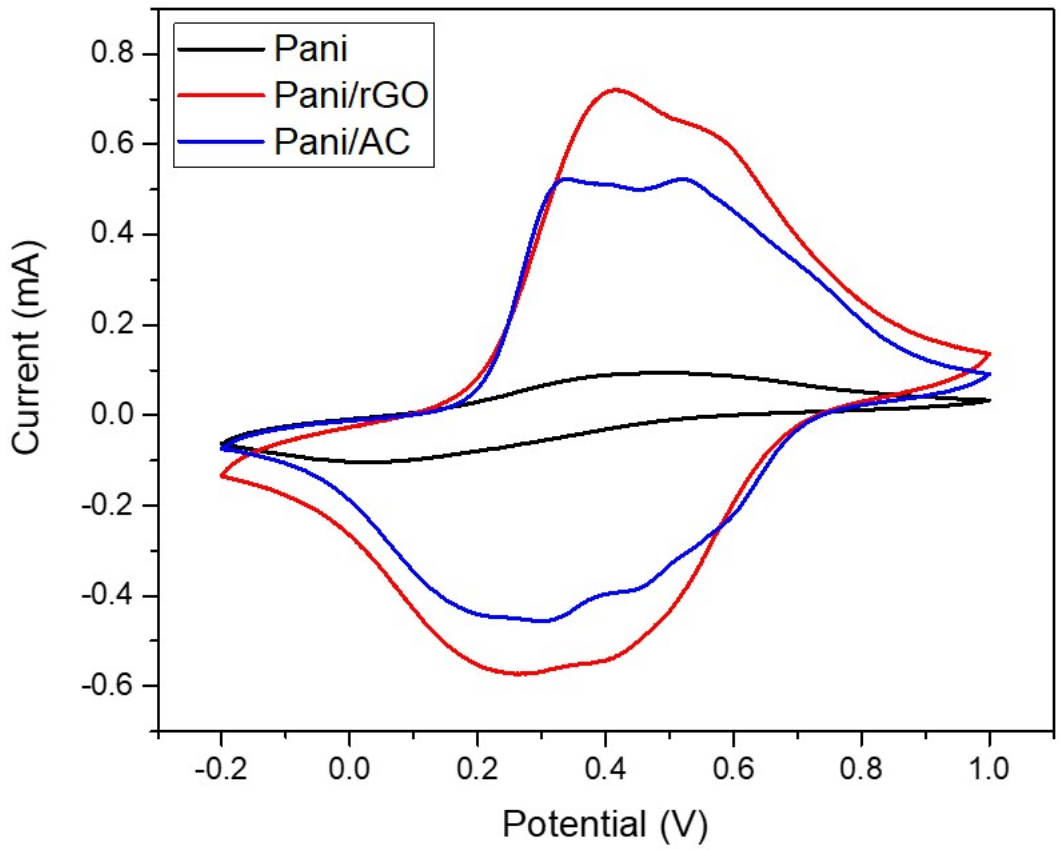

Figure 3. Cyclic voltammogram of Pani, Pani/rGO composite, and Pani/AC composite at a scan rate of 10 mV/s in a 1M H_2SO_4 solution.

The specific capacitance (C_s) was calculated from the CV curve using Equation (1) [24]. The results are shown in Table 2.

$$C_s = \frac{\int I dV}{\Delta V \cdot m \cdot v} \quad (1)$$

where: C_s – specific capacitance [F/g], I – current [A], v – scan rate [mV/s], m – mass [g], V – potential [V].

Table 2. Results of CV measurements of Pani, Pani/rGO, and Pani/AC composites.

Samples	Specific capacitance (C_s), F/g (10mV/s)	Anode b-value	Cathode b-value	b-value Anode/cathode	Capacitance retention rate, %
Pani	19.5	0.624	0.621	1.005	49
Pani/rGO	131.775	0.801	0.706	1.134	51
Pani/AC	105.9	0.756	0.821	0.921	55

The b-value analysis was conducted to assess the kinetic behavior of the samples. The CV was analyzed at various scan rates from 5 to 100 mV/s to determine the kinetic behavior of the samples. The results of the CV measurements are presented in Figure 4 (a-c).

Vol. 66 No 01(257) 2026
https://doi.org/10.5564/pmas.v66i01.5134

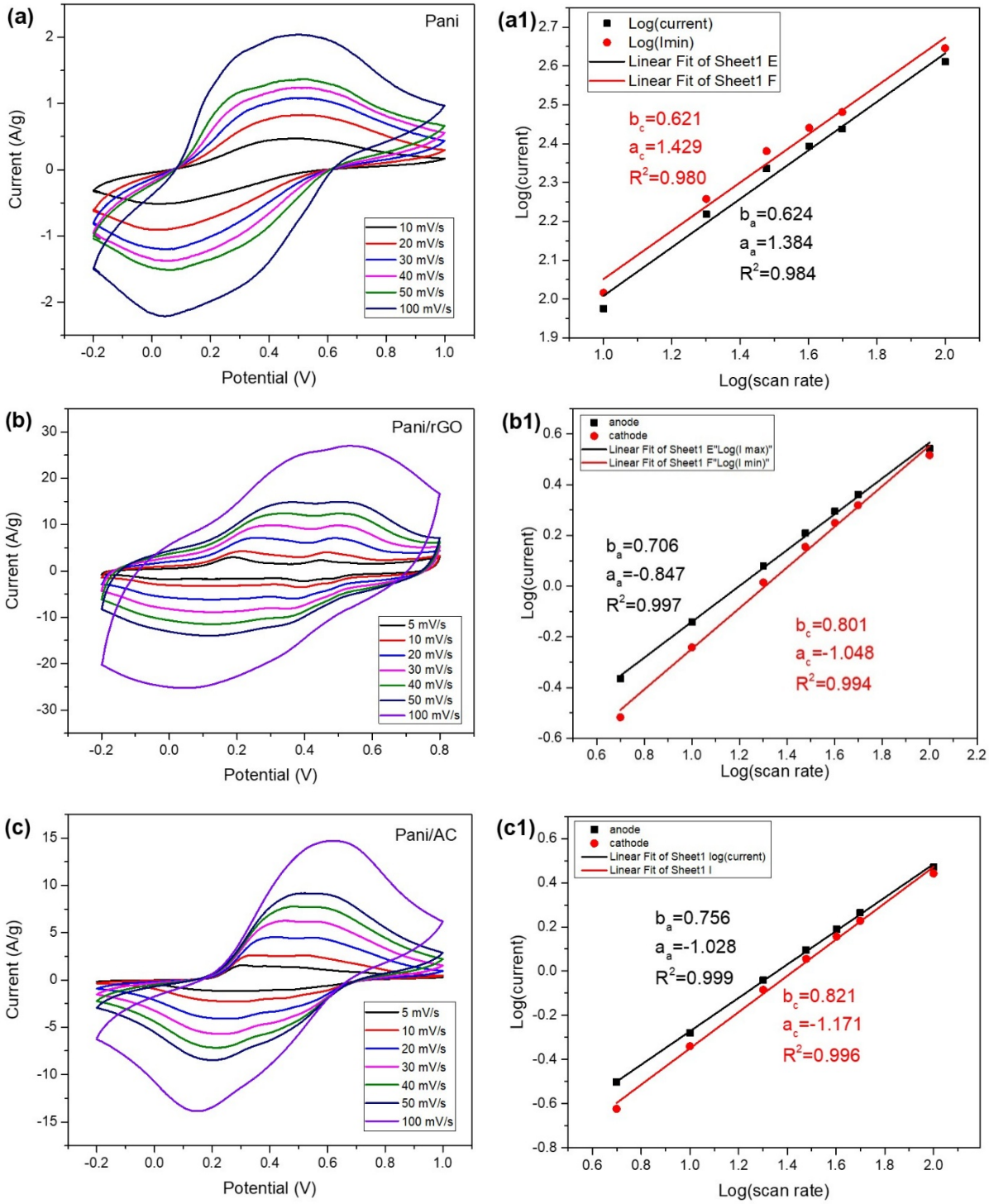

Figure 4. CV curves of (4a) Pani, (4b) Pani/rGO, (4c) Pani/AC composites with different scan rates, and (4a1-4c1) anodic and cathodic log (i_p) vs log(v) plot.

The kinetic mechanism of the electrodes was determined empirically using Equation (2), where the current peak (i_p) versus the scan rate (v) follows a power law. Here, coefficients *a* and *b* are adjustable parameters. To find the coefficients *a* and *b*, Equation (2) can be converted into Equation (3) and derived from the logarithmic linear relationship [25].

$$i_p = av^b \quad (2)$$

$$log(i) = blog(v) + log(a) \quad (3)$$

Vol. 66 No 01(257) 2026
https://doi.org/10.5564/pmas.v66i01.5134

When *b* is equal to 0.5, the current is directly proportional to the square root of the measurement velocity, and diffusion-limited mechanisms dominate the surface. If the *b*-value is equal to or closer to 1, then surface-controlled phenomena occur. On the other hand, when the *b*-value of the electrode falls between 0.5 and 1, it indicates that the electrode exhibits a mixed control kinetic behavior. The *b*-value in Equation (2) for the Pani, Pani/rGO, and Pani/AC composites was determined from Figure 4(a1-c1), and the results are shown in Table 2. The highest *b* coefficient value for the Pani/AC composite sample indicates a high capacitance, with the double-layer capacitance of AC being dominant.

Finally, the capacitance retention rate was calculated, as shown in Figure 5. The specific capacitance of the Pani/rGO composite was higher than that of the Pani/AC composite; however, the capacitance retention rate from measurements at different scan rates indicates that the Pani/AC (55%) composite experiences lower capacitance losses, meaning it operates more quickly and stably.

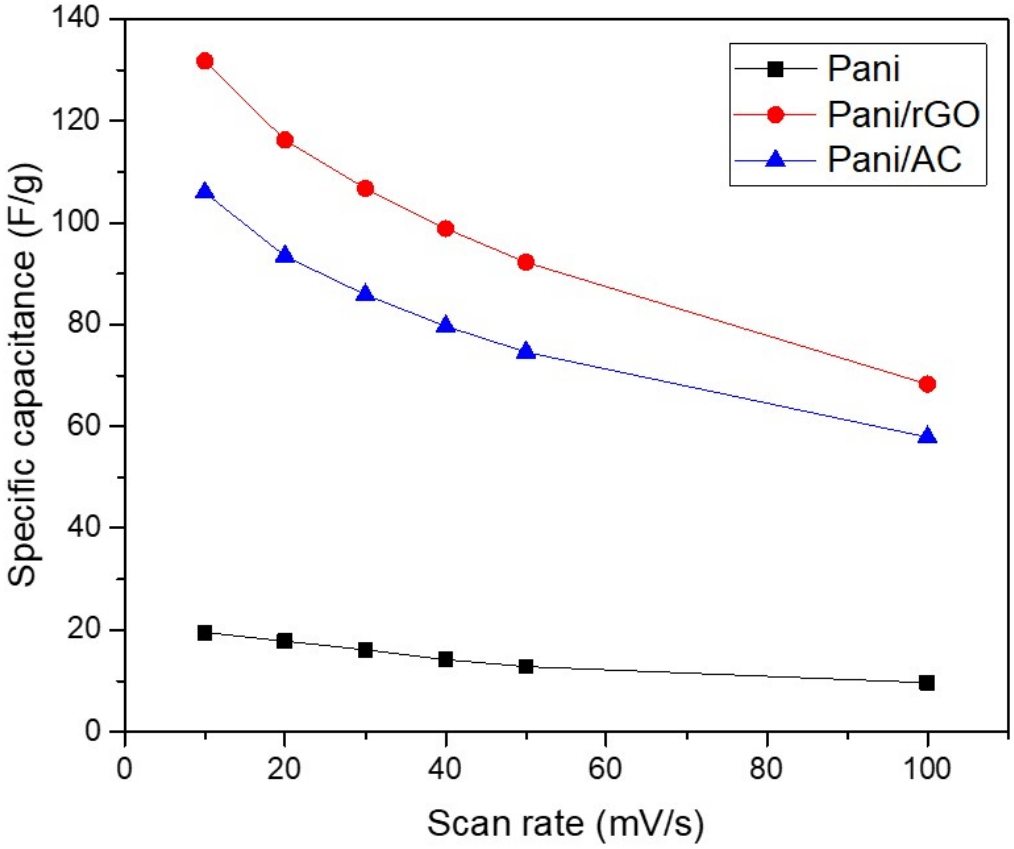

Figure 5. Specific capacitance of Pani, Pani/rGO, and Pani/AC composites with different scan rates.

GCD measurements were performed at a current density of 0.1 A/g (Figure 6a). The specific capacitance was determined from the discharge curve using the formula in [26]. Pani/AC exhibited a higher specific capacitance (181.9 F/g) compared to the Pani (92.6 F/g) and Pani/rGO (145.8 F/g) composites.

In Figure 6b, a Nyquist plot of the EIS measurements wasobtained to determine the charge transfer resistance on the surface. The resistance was low for pure Pani, but high for the composites, which is due to the reduced specific surface area and agglomeration.

Vol. 66 No 01(257) 2026
https://doi.org/10.5564/pmas.v66i01.5134

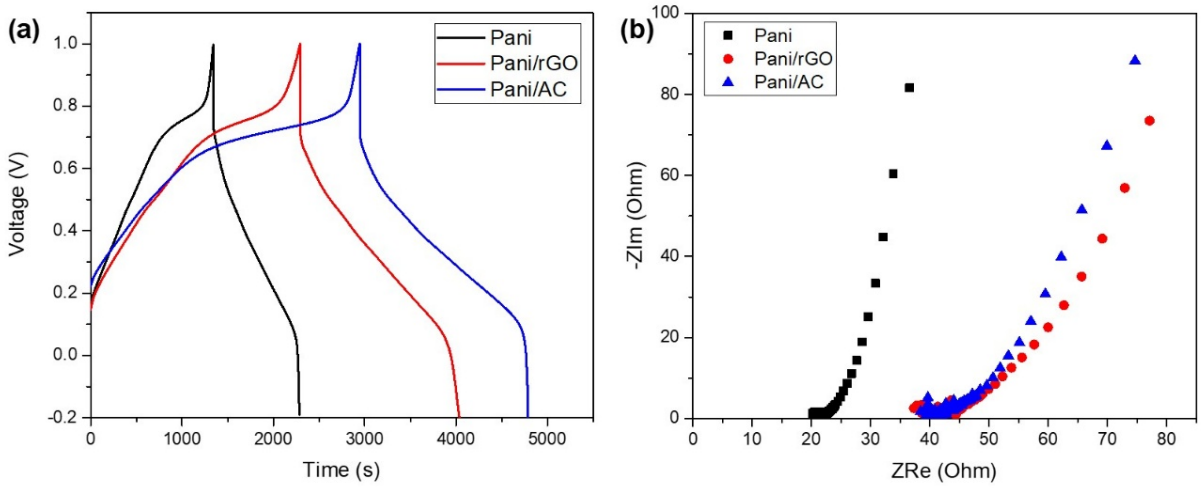

Figure 6. (6a) GCD curve at current density of 0.1A/g, (6b) Nyquist plot of Pani, Pani/rGO, and Pani/AC composites.

Table 3 compares the results with those from previously published works. Our results are lower than those of previously published works. This might be because of the low specific surface area.

Table 3. Comparison of the supercapacitive properties of supercapacitors with those in the literature.

Samples	Electrolyte	Cell voltage, (V)	Current density, (A/g)	Specific capacitance, (F/g)	Ref
PANI/AC nanocomposite	2 M H_2SO_4	-0.6 to 1.0	0.02	66.6	[27]
Bamboo carbon/PANI	1 M H_2SO_4	-0.2 to 0.8	0.5	277	[28]
AC-PANI	2 M H_2SO_4	-0.2 to 1.0	0.1	378	[29]
rGO/PANI	1 M H_2SO_4	-0.2 to 0.8	0.5	397.0	[30]
Pani-NFs/rGO	1 M H_2SO_4	-0.2 to 0.8	1	942.0	[31]
Pani/rGO	1 M H_2SO_4	-0.2 to 1.0	0.1	181.9	This work
Pani/AC		-0.2 to 1.0	0.1	145.8	

Supercapacitor

A symmetrical supercapacitor with a Pani/AC electrode was assembled, and the results were compared with those of the symmetric Pani/rGO//Pani/rGO supercapacitor, studied in previous work by the authors [26].

The CV curves from a symmetric capacitor with a Pani/AC electrode in a 1 M H_2SO_4 electrolyte at scan rates, ranging from 5 to 100 mV/s, are displayed in Figure 7a. As the scan rate increases, the CV curve shape stays consistent, indicating good reversible behavior.

In Figure 7b, the CV curves of the supercapacitors with the Pani/rGO and Pani/AC electrodes at a scan rate of 50 mV/s are compared. The CV curve area of the Pani/AC//Pani/AC composite is larger, and an oxidation peak is observed, compared to the symmetric Pani/rGO//Pani/rGO supercapacitor, indicating that the former is more electrochemically active.

The GCD curves of the supercapacitors with the Pani/rGO and Pani/AC electrodes were compared at a current density of 0.1 A/g (Figure 7c). As demonstrated in this graph, the higher the

Vol. 66 No 01(257) 2026
https://doi.org/10.5564/pmas.v66i01.5134

curve of the Pani/AC composite, the greater the capacitance, and the larger the voltage window compared to the Pani/rGO composite.

From the Nyquist plot in Figure 7d, the symmetric Pani/AC//Pani/AC supercapacitor shows a small semicircle, indicating low charge transfer resistance due to its high surface area, and this porosity does not hinder the charge transfer process.

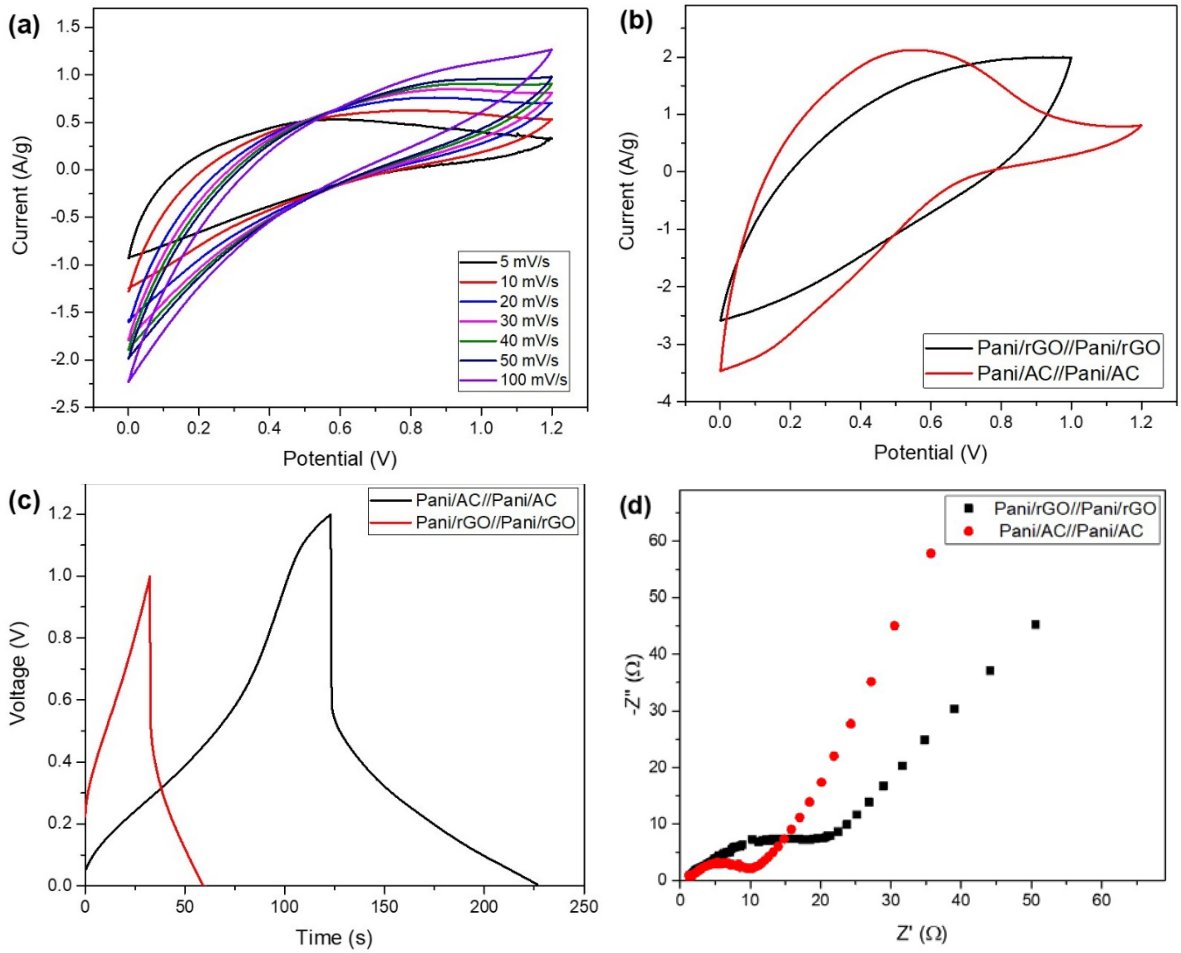

Figure 7. (7a) CV curves of symmetric Pani/AC//Pani/AC supercapacitor with different scan rates, comparison of (7b) CV curves, (7c) GCD curves, (7d) Nyquist plot of symmetric Pani/rGO//Pani/rGO supercapacitor and symmetric Pani/AC//Pani/AC supercapacitor.

Figure 8a shows the GCD measurements of the symmetric Pani/AC//Pani/AC supercapacitor at different current densities, which were used to calculate the energy density and power density to build a Ragone plot (Figure 8c).

The specific capacitance of the symmetric supercapacitor with Pani/rGO and Pani/AC electrodes at different current densities is shown in Figure 8b.

The specific capacitance of the symmetric Pani/AC//Pani/AC supercapacitor was higher. The high charge rate capability of the Pani/AC//Pani/AC supercapacitor was 75.4%, which was greater than that of the Pani/rGO//Pani/rGO supercapacitor (50.5%), indicating it was more stable and capable of carrying a load.

Vol. 66 No 01(257) 2026
https://doi.org/10.5564/pmas.v66i01.5134

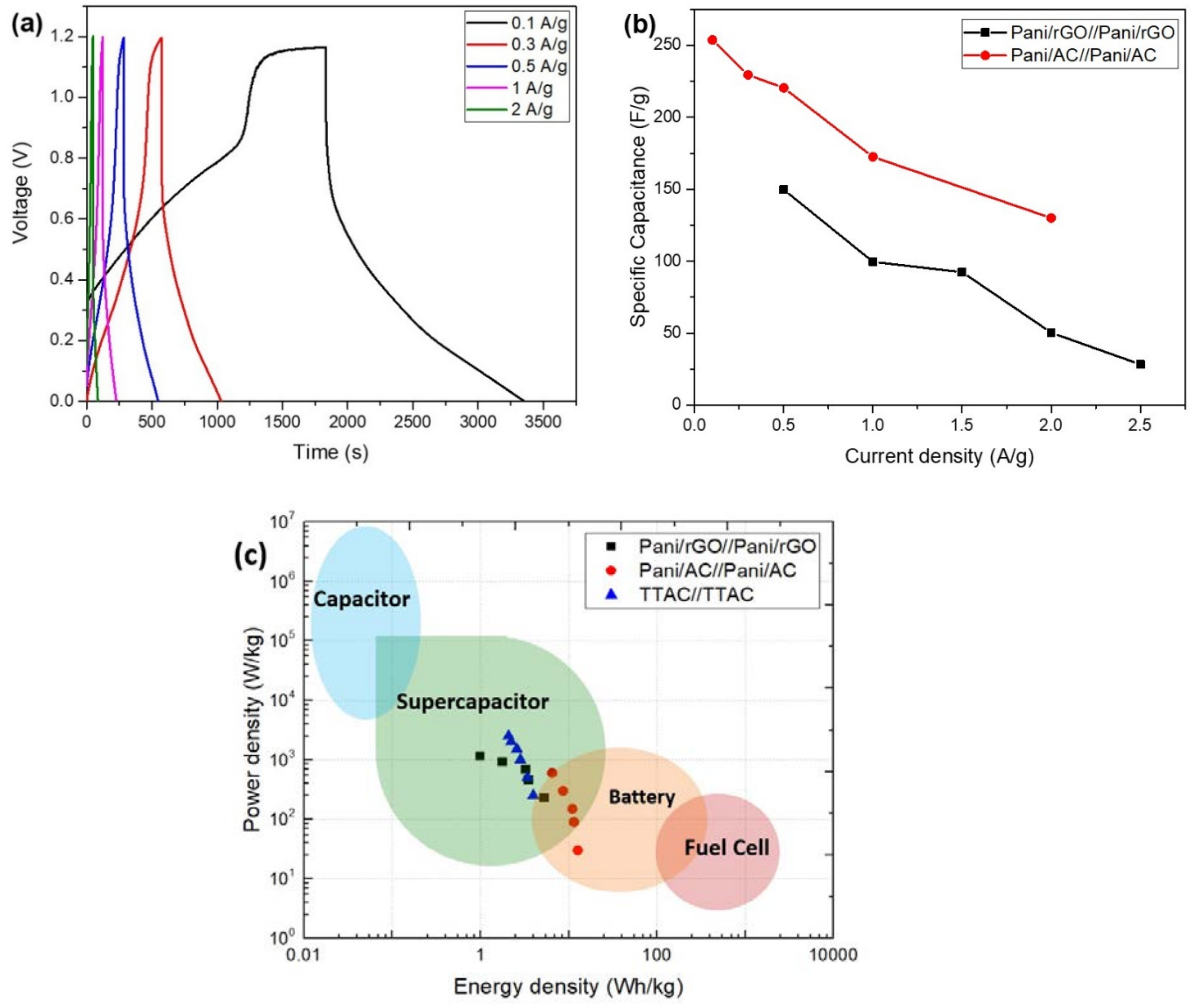

Figure 8. (8a) GCD curves of symmetric Pani/AC//Pani/AC supercapacitor with different current densities, (8b) Comparison of specific capacitance of symmetric Pani/rGO//Pani/rGO supercapacitor and symmetric Pani/AC//Pani/AC supercapacitor with different current densities, (8c) Ragone plot.

Then, the energy density and power density from the discharge curve were calculated, using the formula in [26], and the results were depicted in Figure 8c. For the Pani/rGO composite, at a current of 1 A/g, the energy density is 3.6 Wh/kg, and the power density is 500 W/kg, and for the Pani/AC sample, the energy density at 1 A/g is 6.5 Wh/kg, and the power density is 600 W/kg. The higher energy density of the Pani/AC sample is due to its greater specific capacitance. In addition, characterization results of Mongolian coal-derived activated carbon (TTAC) reported in [32] were compared with those obtained in this study. The coal-derived activated carbon shows comparable properties to the Pani/rGO composites.

CONCLUSIONS

In this study, we compared Pani, Pani/rGO, and Pani/AC composites produced by the polymerization method for application as an electrode material of a supercapacitor. The composite of polyaniline with activated carbon showed impressive results, reaching a maximum specific capacitance of 181.9 F/g and a charge retention rate of 55%. This is because the doped polyaniline with activated carbon has a high specific surface area.

The results showed that the electrochemical activity of the composite materials improves, compared to pure Pani, indicating a synergistic effect between Pani and rGO, and also between Pani and AC.

Vol. 66 No 01(257) 2026
https://doi.org/10.5564/pmas.v66i01.5134

The finding that polyaniline doped with activated carbon is comparable to results obtained with 2D-structured composites suggests the potential for further development of composite samples using activated coal. Significantly, using activated coal to fabricate supercapacitor electrodes, as described, has the potential to generate yet another revenue stream for Mongolia's abundant coal resources.

Ethical approval

There are no ethical issues with the publication of this article.

Author contribution

The authors confirm contribution to the paper as follows: BoB- writing original draft, data curation, visualization, and computing. BuB- methodology, review and editing, conceptualization. NB- data curation. SG: writing, review and editing. All authors reviewed the results and approved the final version of the article.

Conflict of Interest

The authors declare no conflict of interest.

REFERENCES

1. W. Du, et al., Nitrogen-doped hierarchical porous carbon using biomass-derived activated carbon/carbonized polyaniline composites for supercapacitor electrodes, Journal of Electroanalytical Chemistry 827 (2018) 213-220. https://doi.org/10.1016/j.jelechem.2018.09.031.
2. G. Yu, et al., Hybrid nanostructured materials for high-performance electrochemical capacitors, Nano Energy 2 (2013) 213-234. https://doi.org/10.1016/j.nanoen.2012.10.006.
3. P. Forouzandeh, et al., Electrode Materials for Supercapacitors: A Review of Recent Advances, Catalysts 10 (2020) 969. https://doi.org/10.3390/catal10090969.
4. H. Wang, et al., Polyaniline (PANi) based electrode materials for energy storage and conversion, Journal of Science: Advanced Materials and Devices 1 (2016) 225-255. https://doi.org/10.1016/j.jsamd.2016.08.001.
5. B. Bumaa, et al., Evolution of electrochemical properties of polyaniline doped by graphene oxide, Polymer Bulletin 79 (2022) 7443-7458. https://doi.org/10.1007/s00289-021-03837-0.
6. H. Gul, et al., Study on Direct Synthesis of Energy Efficient Multifunctional Polyaniline–Graphene Oxide Nanocomposite and Its Application in Aqueous Symmetric Supercapacitor Devices, Nanomaterials 10 (2020) 118. https://doi.org/10.3390/nano10010118.
7. M. Yanilmaza, et al., Flexible polyaniline-carbon nanofiber supercapacitor electrodes, Journal of Energy Storage 24 (2019) 100766 https://doi.org/10.1016/j.est.2019.100766.
8. Pal R, et al., Efficient energy storage performance of electrochemical supercapacitors based on polyaniline/graphene nanocomposite electrodes, Journal of Physics and Chemistry of Solids 154 (2021) 110057. https://doi.org/10.1016/j.jpcs.2021.110057.
9. Gui D, et al., Preparation of polyaniline/graphene oxide nanocomposite for the application of supercapacitor, Applied Surface Science 307 (2014) 172–177. https://doi.org/10.1016/j.apsusc.2014.04.007
10. Luo J, et al., Preparation of morphology-controllable polyaniline and polyaniline/graphene hydrogels for high-performance binder-free supercapacitor electrodes, Journal of Power Sources 319 (2016) 73–81. https://doi.org/10.1016/j.jpowsour.2016.04.004.
11. Qin G, et al., Novel graphene nanosheet-

wrapped polyaniline rectangular-like nanotubes for flexible all-solid-state supercapacitors, Journal of Materials Science 52 (2017) 10981–10992. https://doi.org/10.1007/s10853-017-1273-5.

12. Q. Zhang, et al., Electropolymerization of graphene oxide/polyaniline composite for high-performance supercapacitor, Electrochimica Acta 90 (2013) 95-100. https://doi.org/10.1016/j.electacta.2012.11.035.
13. N. A. Kumar, et al., Polyaniline-grafted reduced graphene oxide for efficient electrochemical supercapacitors, ACS Nano 6 (2012) 1715-1723. https://doi.org/10.1021/nn204688c.
14. Z. Zhao, et al., Facile fabrication of binder-free reduced graphene oxide/MnO2/Ni foam hybrid electrode for high-performance supercapacitors, Journal of Alloys and Compounds 812 (2020) 152124. https://doi.org/10.1016/j.jallcom.2019.152124.
15. K. Jin, et al., In–situ hybridization of polyaniline nanofibers on functionalized reduced graphene oxide films for high-performance supercapacitor, Electrochimica Acta 285 (2018) 221-229. https://doi.org/10.1016/j.electacta.2018.07.220.
16. G. Singh, et al., Improved electrochemical performance of symmetric polyaniline/activated carbon hybrid for high supercapacitance: Comparison with indirect capacitance, Polymers for Advanced Technologies 32 (2021) 4490-4501. https://doi.org/10.1002/pat.5451.
17. N. Mahato, et al., Semi-Polycrystalline Polyaniline-Activated Carbon Composite for Supercapacitor Application, Molecules 28 (2023) 1520. https://doi.org/10.3390/molecules28041520.
18. N. Yang, et al., Polyaniline-modified renewable biocarbon composites as an efficient hybrid electrode for supercapacitors, Ionics 25 (2019) 5459-5472. https://doi.org/10.1007/s11581-019-03063-9.
19. B. Bumaa, et al., Enhanced polyaniline composites for supercapacitor applications, Journal of Electronic Materials 51 (2022) 5134-5141. https://doi.org/10.1007/s11664-022-09768-4.
20. S. N. Alam, et al., Synthesis of Graphene Oxide (GO) by Modified Hummers Method and Its Thermal Reduction to Obtain Reduced Graphene Oxide (rGO)*, Graphene 6 (2017) 1-18. https://doi.org/10.4236/graphene.2017.61001.
21. Y. Zhang, et al., Facile synthesis of hierarchical nanocomposites of aligned polyaniline nanorods on reduced graphene oxide nanosheets for microwave absorbing materials, RSC Advances 7 (2017) 54031–54038. https://doi.org/10.1039/C7RA08794B.
22. N. Chen, et al., In situ one-pot preparation of reduced graphene oxide/polyaniline composite for high-performance electrochemical capacitors, Applied Surface Science, 392 (2017) 71-79. https://doi.org/10.1016/j.apsusc.2016.07.168.
23. S.Xiong, et al., One-pot hydrothermal synthesis of polyaniline nanofibers/reduced graphene oxide nanocomposites and their supercapacitive properties, High Performance Polymers 31 (2019) 1238-1247. https://doi.org/10.1177/0954008319845435
24. T. S. Mathis, et al., Energy Storage Data Reporting in Perspective-Guidelines for Interpreting the Performance of Electrochemical Energy Storage Systems, Advanced Energy Materials 9 (2019) 1902007. https://doi.org/10.1002/aenm.201902007.
25. H. Rueda, et al., Production of a nickel-based catalyst for urea electrooxidation using spent batteries as raw material: Electrochemical synthesis and implications from a circular economy stand-point, Sustainable Materials and

Vol. 66 No 01(257) 2026
https://doi.org/10.5564/pmas.v66i01.5134

Technologies 29 (2021) e00296. https://doi.org/10.1016/j.susmat.2021.e00296.
26. B. Bolormaa, et al., Polyaniline/reduced grapheneoxide composite as an electrode for symmetric and asymmetric supercapacitors, Journal of Applied Polymer Science, 142 (2025) e56785. https://doi.org/10.1002/app.56785.
27. A. Olad, et al., Study on the capacitive performance of polyaniline/activated carbon nanocomposite for supercapacitor application, Journal of Polymer Research 23 (2016). https://doi.org/10.1007/s10965-016-1031-4.
28. X. Zhou, et al., A renewable bamboo carbon/polyaniline composite for a high-performance supercapacitor electrode material, Journal of Solid State Electrochemistry 16 (2012) 877–882. https://doi.org/10.1007/s10008-011-1435-3.
29. A. Olad, et al., Preparation and electrochemical investigation of the polyaniline/activated carbon nanocomposite for supercapacitor applications, Progress in Organic Coatings 81 (2015) 19-26. https://doi.org/10.1016/j.porgcoat.2014.12.009.
30. N. Chen, et al., In situ one-pot preparation of reduced graphene oxide/polyaniline composite for high-performance electrochemical capacitors, Applied Surface Science, 392 (2017) 71-79. https://doi.org/10.1016/j.apsusc.2016.07.168.
31. S. Xiong, et al., One-pot hydrothermal synthesis of polyaniline nanofibers/reduced graphene oxide nanocomposites and their supercapacitive properties, High Performance Polymers, 31 (2019) 1238-1247. https://doi.org/10.1177/0954008319845435.
32. B. Bolormaa, et al., Potential of Coal-Derived Activated Carbon as an Electrode Material for Supercapacitors, Journal of Khureltogoot, (2025), vol. 21, pp. 82-85.